ELSEVIER

Contents lists available at ScienceDirect

### **Applied Thermal Engineering**

journal homepage: www.elsevier.com/locate/apthermeng



#### Research Paper



## Cooling of electronic circuits through elastocaloric solid-state technology: A numerical analysis for the development of the CHECK TEMPERATURE prototype

Claudia Masselli<sup>\*</sup>, Luca Cirillo, Adriana Greco

Department of Industrial Engineering (DII), University of Naples Federico II, Piazzale Tecchio 80, 80125 Naples, Italy

#### ARTICLE INFO

# Keywords: Elastocaloric effect Shape-memory alloys Solid-state refrigerants Caloric refrigeration Not-In-Kind-cooling technologies Cooling of electronic circuits Experimental prototype

#### ABSTRACT

Elastocaloric technology represents a valid environmentally friendly proposal, among the cooling technologies alternative to vapor compression. Elastocaloric cooling is based on solid state materials exhibiting elastoCaloric Effect. The phenomenon, detected in shape memory alloys, is visible in a temperature change generated by the variation of the intensity of an external mechanical field. CHECK TEMPERATURE is a project aiming at developing a smart elastocaloric device for cooling of electronic circuits. It has the aim to develop the first elastocaloric device for electronic circuits cooling. In this paper a numerical analysis for the development of the CHECK TEMPERATURE prototype is presented. The device is formed by multiples arrays of 240 wires of Ni<sub>50.8</sub>Ti<sub>49.2</sub> alloy that favourably works in room temperature range. The mechanism for loading/unloading the wires is bending whereas air is the heat transfer fluid flowing in the channels. The investigation is carried out by means of a 2D numerical model through which optimizing both the geometrical configuration for the assembly of the elastocaloric material in the channel and the working conditions. The lengths and the placement of the wires along the channels have been investigated over variable values of cycle frequency and air flow speed. 0.5 mm as distance between two wires having a length of 20 cm is the best solution that, keeping constant the number of wires, allows to employ 30 % less elastocaloric material with consequent cost saving, giving at the same time satisfactory energy performances (6.5 as COP, 23.8 K as global temperature span).

#### 1. Introduction

#### 1.1. Problem background

The elastoCaloric (eC) cooling is defined as a Not-In-Kind Refrigeration Technology [1] and, more specifically, belongs to the class of the Solid-State ones based on caloric effects [2]. The latter is recognized as possible replacement for Vapor Compression (VC) [3,4]. Currently VC systems contributes for 20 % to the worldwide energy demand. The well-known Montreal [5] and Kyoto Protocols [6] in 1987 and 1997 have established prescriptions for mitigating the environmental impact caused by the refrigerants that VC has been basing on. From 1996 in Europe the usage of ChloroFluoroCarbons (CFCs) and Hydro-ChloroFluoroCarbons (HCFCs), exhibit elevate Ozone Depletion Potential (ODP) and Global Warming Potential (GWP) values, was forbidden [7–9]. Subsequent prescriptions fixed stringent margins [10] toward the increasingly phasing out from 2015 of the HydroFluoroCarbons (HFCs)

with the goal of getting, in 2036, the 85 % of the whole dismission. HydroFluoroOlefins (HFOs) are the most accredited refrigerants as dropin [11,12] but anyhow they are expensive and due of a trivial flammability, that can avoid the reaching of the safety standards required by some applications.

The above-introduced scenario constitutes a very strong impulse towards the identification and development of innovative refrigeration techniques that can respond to requirements of both environmental preservation and energy eco-sustainability. Next to the renewable energy-sources-based systems (e.g. geothermal, solar...) [13,14], among the various emerging proposals appearing in scientific literature, the class of solid-state refrigeration techniques based on the caloric effect assumes certain relevance [15]. The main foundations in the bet towards solid state refrigeration can be traced back to: i) the zero-GWP and zero-ODP feature proper of the solid-state materials employed as caloric refrigerants, as well as the non-flammability, non-toxicity, non-explosiveness [1,3,4]; ii) the  $+50\,\%$  as increment of energy performances shown by caloric systems with respect to VCs [2–4]; iii) the

E-mail address: claudia.masselli@unina.it (C. Masselli).

<sup>\*</sup> Corresponding author.

Nomenclature		δ	infinitesimal difference, -
		ε	strain, N
Roman symbols		$\overline{arepsilon}$	Infinitesimal quantity, -
Α	Austenite phase temperature, °C	υ	cinematic viscosity, m <sup>2</sup> s <sup>-1</sup>
a	grouping factor, -	ξ	phase fraction, -
an	square wave function, -	έ	instantaneous phase fraction, s <sup>-1</sup>
В	Boltzmann constant, m <sup>2</sup> kg s <sup>-2</sup> K <sup>-1</sup>	ρ	density, kg m <sup>-3</sup>
b	grouping factor, -	σ	uniaxial stress, MPa
Bi	Biot number, -	τ	convective heat exchange transient constant, s
c	specific heat capacity, $J kg^{-1} K^{-1}$	Ψ	probability, -
D	diameter, mm	•	
d	space between two wires, mm	Subscript	
E	Young modulus, MPa	0	Initial
f	frequency, Hz	1	Final
g	elastocaloric term, W m <sup>-3</sup>	A	Austenite
H	Latent heat, J g <sup>-1</sup>	AM	Austenite-to-Martensite transformation
h	convective heat transfer coefficient, W $m^{-2}$ K <sup>-1</sup>	ad	adiabatic
k	thermal conductivity, $W m^{-1} K^{-1}$	air	air
L	length of the wire, mm	bend	bending
M	Martensite phase temperature, °C	CHANNI	EL on the single channel
m	Mass, kg	CHECK	on the whole device
ṁ	flow rate, kg s <sup>-1</sup>	cool	cooling
n	number of times	cycle	cycle
p	pressure, Pa	env	environment
Q	thermal power, W	f	finish
S	entropy, J $kg^{-1}$ $K^{-1}$	inlet	inlet
Surf	Surface area, m <sup>2</sup>	load	loading
T	Temperature, K	M	Martensite
t	time, s	MA	Martensite-to-Austenite transformation
u	x-velocity field component, m s <sup>-1</sup>	MAX	maximum
V	volume, m <sup>3</sup>	net	net
v	y-velocity field component, m s <sup>-1</sup>	outlet	outlet
		p	constant pressure
$\overrightarrow{v}$	velocity vector, m s <sup>-1</sup>	S	start
W	loading/unloading work, J g <sup>-1</sup>	SMA	Shape Memory Alloy
X	longitudinal spatial coordinate, m	span	span
X	Conjugate field	unload	unloading
y	orthogonal spatial coordinate, m	wire	single wire
Y	Driving field	x	along x-coordinate
Greek s	vmbols		-
Δ	finite difference, -		
_			

consequent lower Total Equivalent Warming Impact (TEWI) values compared to VCs [3] coming from the advantages reported in points i) and ii). This makes caloric cooling an advanced technology for future and the design and manufacturing of sustainable performing prototypes can represent a turning point in the history of this field.

#### 1.2. Physical phenomenon and thermodynamic cycles

All the technologies belonging to solid-state caloric systems found on different-nature caloric materials and effects that can be generated by magnetic, electric, mechanical or pressure forcing fields, respectively proper of magnetocaloric [16–23], electrocaloric [24–26], elastocaloric [27–29] or barocaloric [30] cooling. The phenomenon of caloric effect can be globally illustrated as the observation of a temperature change  $(\Delta T_{ad})$  in the solid-material due to an intensity-changing field (Y) forcing it under adiabatic conditions:

$$\Delta T_{ad} = -\int_{Y_0}^{Y_1} \frac{T}{C} \left( \frac{\partial X}{\partial T} \right)_Y dY \tag{1}$$

Dually in an isothermal process, a change in the forcing field can generate a variation of the total entropy of the material:

$$\Delta S = \int_{Y_0}^{Y_1} \left(\frac{\partial X}{\partial T}\right)_Y dY \tag{2}$$

Y and X are the forcing and the coupled fields, respectively. Regarding the elastoCaloric Effect (eCE), Y =  $\sigma$  (stress) and X =  $\epsilon$  (strain).

Going through the specific concepts related to the elastocaloric technology, eCE is a phenomenon detectable in materials categorized as Shape Memory Alloys (SMA) [31] with the capabilities of shape-memory and superelasticity. The first one means that an elastocaloric materials can remind its initial shape (even if it is stressed), so memorizing the possibility of reshaping after the stress remotion; whereas superelasticity provides the possibility by the SMA to suffer elevate strains (up to 9 %) and the releasement/absorption of its latent heat during the phase change. Every SMA can be in Austenite (A) or Martensite (M) structural phase and the transitions A-to-M or M-to-A occur as a consequence of loading and unloading operations. When a SMA is in the austenite phase and a stress is applied (loading) is enough to guarantee the austenite-to-martensite transition greater than the A-to-M saturation stress, identified as  $\sigma_{AM}(T)$ ), an exothermic process occurs. If the transformation is isothermal, a certain amount of heat is released; if the

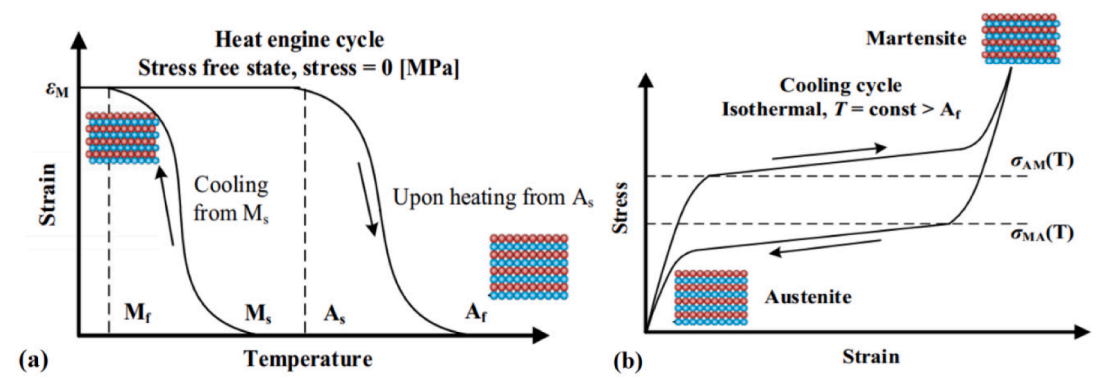


Fig. 1. The elastocaloric cycles for SMAs: (a) the direct thermally driven; (b) the inverse stress-driven.

material is stressed adiabatically, the material heats up. Dually, the remotion of the stress (unloading) below the *M-to-A saturation stress* ( $\sigma_{MA}(T)$ ), generates the reverse transformation (Martensite to Austenite) and an endothermic process takes place. If the transformation is adiabatic, the SMA cools down and it decreases its temperature; if the transformation is isothermal a certain amount of heat is absorbed. The intensity of the eCE is related on the loading intensity and on whole amount of the latent heat characterizing the complete adiabatic transformation of the structural phases (martensite/austenite) [32]. The latter represents an upper limit translating in a maximum observable  $\Delta T_{ad}$ . A-M and M-A processes are characterized by thermal hysteresis:  $\sigma_{AM}$  and  $\sigma_{MA}$  are not coincident, as well as the transition temperatures ( $A_f$ ,  $A_s$ ,  $M_f$ ,  $M_s$ ).

The above-mentioned behaviour of the elastocaloric SMAs allows to design two kinds of thermodynamic cycles: the direct thermally driven cycle (e.g. for a heat engine) and the inverse stress-driven cycle (e.g. exploitable for a cooling or heating pump system), that are illustrated in Fig. 1(a) and (b), respectively.

As visible from Fig. 1(a) the direct thermally driven cycle is representative for the heat engine operation, i.e. the conversion of heat into a strain change together with the dissipation of heat toward a low temperature heat sink. Following the path displayed in Fig. 1(a) the cycle begins with the SMA below  $M_f$ . A heat is adduced to the eC material and the temperature starts to rise. Once the temperature touches  $A_s$ , the M-A transformation begins, and it ends when the quantity of heat adduced is enough to carry the SMA at  $A_f$ . Then the reverse cooling operation starts and the SMA is austenite above  $M_s$ . Subsequently the A-M transformation occurs with a temperature reduction down to  $M_f$ .

Dually, in Fig. 1(b) the inverse stress-driven cycle that begins with no stress applied and the SMA in austenite phase is illustrated. The application of a stress level greater than  $\sigma_{AM}$ , under adiabatic conditions, gives rise to the A-M transition, the elastocaloric effect occurs and the SMA increases its temperature. Conversely the stress is adiabatically decreased below the threshold level  $\sigma_{MA}$  and the SMA starts to transform itself in austenite and consequently a temperature reduction is observed since the elastocaloric effect is manifesting.

The inverse stress-driven cycle can be employed in many well-known thermodynamical cycles for controlling the behaviour of a cooling system [33]. The most used cycle for eC refrigeration is the reverse Brayton-based one with regeneration called AeR cycle, that is the acronym of Active elastocaloric Regenerative refrigeration cycle. In an AeR-based system the elastocaloric SMA has also the function of regeneration and a secondary fluid has the role of heat transfer vector. The operation of regeneration allows to recover an amount of heat that in a single stage cycle would be lost. It allows the AeR cycle to guarantee a temperature span across the regenerator that is greater than the  $\Delta T_{\rm ad}$  (that is proper of the material itself and only to eCE). Without regeneration the  $\Delta T_{\rm ad}$  represents an upper limit in the maximum temperature span detectable in the regenerator. According to Fig. 2 the functioning of the AeR cycle

can be described as follows.

The elastocaloric material is: i) loaded (temperature rising for eCE); then ii) crossed by a Heat Transfer fluid (HTF) to release heat; iii) unloaded (temperature falling for eCE) and then iv) crossed by cold HTF to absorb heat from thermal load.

In Fig. 3 there is another configuration where the heat transfer is executed through a solid material.

In (I) the SMA is loaded and it increases the temperature from T to T +  $\Delta T_{ad,load}.$  (II) is the Heat transfer process where the SMA reduces its temperature thanks to a heat releasing toward a hot sink, occurring through a conductive transfer with a solid material. (III) is the unloading process that is responsible for a further temperature reduction in the SMA (- $\Delta T_{ad,unload}$ ) due to eCE. (IV)the contact between the elastocaloric material and the cold side realizes the absorption of heat from thermal load. This configuration, since it is single stage, allows to reach temperature span up to the adiabatic temperature changes of the material. Further upgrading such as multistage, cascaded or/and regenerative configuration can return a temperature span in the system that is higher than the adiabatic temperature change of the elastocaloric material employed.

There are advanced applications based on Solid-to-Solid Heat Transfer (SSHT) based cycle where rather than the motion of the solid material, the heat transfer processes are regulated by thermal switches that are materials able to change their thermal conductivity as a consequence of the intensity of the field applied to them [34,35].

In this paper the adopted configuration for the analysis is the one shown in Fig. 2.

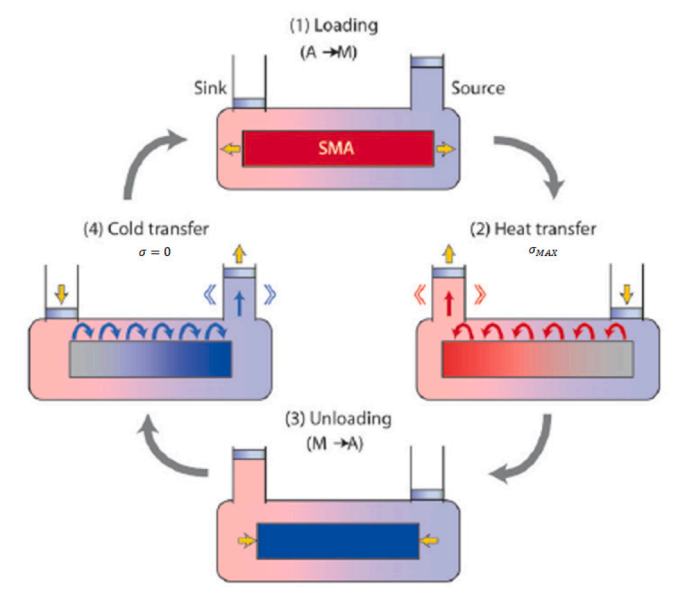


Fig. 2. The AeR cooling cycle.

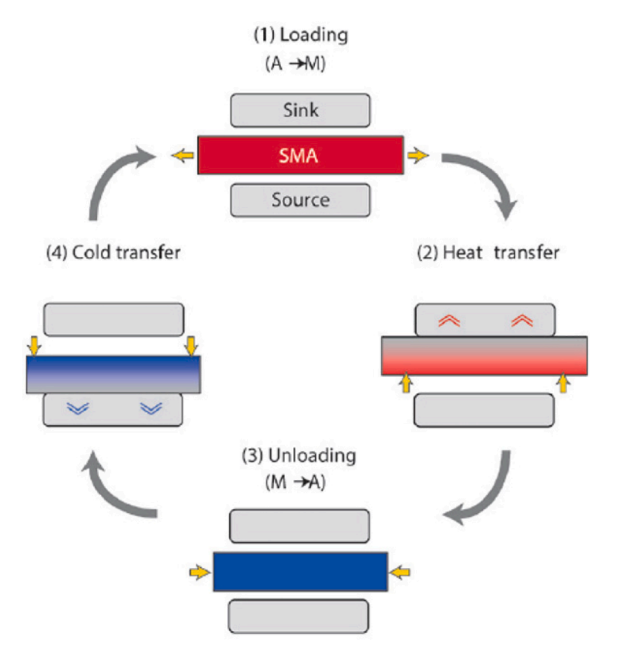


Fig. 3. The solid-to-solid heat transfer based cycle.

#### 1.3. State of the art and research gap

The pioneer and currently the most consolidated and investigated of the four solid-state technologies is the magnetocaloric one. The pushing point toward this research was the magnetocaloric effect shown by Gadolinium in a temperature range compatible with refrigeration applications. So it turned on the spotlights by scientific community on the possibility to conceive a magnetocaloric system for this purpose [36]. The first device, a magnetic heat pump, was developed in 1976 in Ohio (USA) by the National Aeronautics and Space Administration [37]. It was both a begin of the magnetocaloric cooling research and a turning point of the more general research in refrigeration field; currently, more than 100 are the realized devices but none has been commercially produced, yet [38]. The major limitations lay in: i) interesting energy performances but not sufficient for the commercialization [39]; ii) the very expensive magnetocaloric materials (belonging to the rare earth elements) [40]; iii) the low achievable magnetic field intensities with permanent magnets [41].

The spotlight on elastocaloric refrigeration has turned on 10 years ago and scientists devoted their efforts toward: a) new promising materials suitable for cooling and heat pumping purposes; b) projecting and manufacturing of the devices. Also, the modelling plays a relevant role, since it is coupled to the branch of device realization to support in the optimization.

a) Nickel Titanium is the benchmark most studied and employed elastocaloric material.  $\Delta T_{\rm ad}$  shown by the binary alloy touches 25.5 K and 17 K for 5 % strain (loading and unloading) [42,43], even if it can suffer up to 9 % strain. Furthermore, the other advantages exhibited by the binary alloy are the pronounced shape memory properties, the wide availability on the market, and the acceptable fatigue-life for eC applications. The latter is a crucial aspect since a small fatigue-life material has a limited durability in a long operation time. Ni-Ti alloys composed by 3 or 4 elements can help in hysteresis reducing or improving the fatigue life [44]. In 2015 Chluba et al. [45] tested and demonstrated that the addition of Cu to Ni-Ti alloys can provide up to 10  $^7$  loading/unloading cycles before the appearance of cracks. Cu- and Fe-based alloys were also employed in eC processes thanks to their lower costs and the possibility of eCE manifesting under stress values lower than the NiTi-based alloys. The

highest  $\Delta T_{ad}$  detected in Cu-alloys is 15 K under 130 MPa as stress (proper of  $Cu_{68.1}Zn_{15.8}Al_{16}$ ), whereas 5 K is the maximum registered for the Fe-based ones [46]. An emerging class of elastocaloric materials is the one of Shape Memory Polymer (SMP), also embracing natural or synthetic rubbers [47–49]. The main disadvantage of the rubbers is the enormous elongation needed for eCE manifesting (strain corresponding to up to 600 % of the unloaded length).

b) At the best of our knowledge the number of elastocaloric devices realized in laboratory up to 2023 is slightly over the fifteen: some of them experiment the AeR cycle, other ones the solid-to-solid cycle. A part of the is forced by linear drivers, few of others are rotary. The first eC device was introduced in 2012 by Cui et al. [50], a rotary device formed by two rings through where the NiTi wires were fixed. 17 K was the highest temperature span registered but, because of the assembly of the device, the lifetime of the refrigerant was very limited because of the easiness in cracks. In 2019 Greco et al [38] and Kabirifar et al [51] reviewed the eC devices realized. Among them, interesting was another rotary manufacturer [52] employing the quaternary Ni<sub>45</sub>Ti<sub>47.25</sub>Cu<sub>5</sub>V<sub>2.75</sub> to improve the duration of the materials. The previously mentioned were devices oriented toward the air conditioning or heat pumping but also other smaller size elastocaloric devices where developed.

Worthy of mention is the bridge system designed by Bruederlin et al. [53] where the presence of HTF was not required since a slice of elastocaloric material is loaded through bending and, at the same time, moved up and down. The device was then updated [54] with the employment of a a TiNiFe slice as refrigerant. The microscale cooler introduced by Snodgrass and Erickson [55] in 2019 showed the highest temperature span (28.9 K) through the cyclical stretching of few Ni-Ti wires. Parallelly, Ossmer et al [56] presented a miniaturized elastocaloric cooler able to achieve 2.9 W g $^{-1}$  as cooling power and 3.2 as coefficient of performance.

The latest developed elastocaloric devices have been presented in 2022, respectively by Xi'an Jiaotong University [57], University of Ljubljana [58], Technical University of Denmark in collaboration with the German Fraunhofer Institute for Physical Measurement Techniques [59], University of Maryland [60]. The elastocaloric refrigerants employed in, are materials proper of the binary NiTi alloy, with different compositions. The Chinese prototype [57] is linear tensile with air as heat transfer fluid and it is able to achieve 9.2 K as maximum temperature span. The other three are all compression-loading based where water circulates as HTF. The maximum temperature span was 31.3 K and it was achieved by the Slovenian device [58] (mounting tubes of Ni<sub>55.8</sub>Ti<sub>44.2</sub>), that is the highest value ever at the best of our knowledge. On the other side, the peculiarity of the DTU device [59] is to show a promising 1071 W kg<sup>-1</sup>, as specific cooling power, measured by employing tubes of Ni<sub>56,25</sub>Ti<sub>43,75</sub> in an AeR cycle. The prototype designed and realized [60] by the University of Maryland is linear alternate mounting a staggered tube of Ni<sub>50.5</sub>Ti<sub>49.5</sub>. The maximum detected temperature span is 16.6 K whereas no data about cooling power or COP were provided, yet.

From the state of the art, one can notice that many steps have to be taken yet for the production of an elastocaloric device on large scale. One of the reasons is the duration of the eC materials employed and so of the whole device. The most explored fields of applications are the heat pump and refrigeration.

The bottleneck of the eC technology is the short fatigue life of the eC materials that couples with the type of loading applied (to make eCE manifesting in the AeR cycle) but also the achievement of satisfactory operative conditions. The dimensions and the operative conditions of the devices can be optimized through modelling. Most of the eC models developed are 1D [27], apart the ones realized by Cirillo et al [61,62] where a bunch of wires was two-dimensionally analyzed.

With respect to the type of loading applied, due to the mechanical solicitations to which the material is subjected during the cycles of loading/unloading, it is inevitable that after a certain time due to wear, cracks may occur. In Fig. 4 the main ways to load the elastocaloric materials are reported.

The disadvantage of tension is the crack propagation during loading unloading cycles. The disadvantage of compression is the reduction of the available heat transfer surface through compression [63]. However, despite the considerable number of studies on the fatigue life of SMAs (mostly the binary NiTi alloy) subjected to tension, much less are the ones studying their fatigue life in compression. For example, studies show that, applying loading though tension, a durable operation (10<sup>5</sup> cycles) can be achieved in the NiTi alloy with strains around 2 %, which thus corresponds to relatively small  $\Delta T_{ad}$ . The first studies on NiTi cylinders and cubes under compression confirmed a significant improvement compared to tension, with the possibility of reaching up to 70 million loading/unloading cycles [64,65]. Furthermore, alternatively to compression and tension, a recent study [66] focused on torsion, demonstrating a remarkable increasing in lifetime of the material even if smaller are the adiabatic temperature change achievable. Bending seems to be a good answer both to the problem of cracks and satisfactory temperature changes. Sharar et al. [67] found that axisymmetric bending enables a fivefold reduction in the required force for equivalent COP and temperature span, which directly corresponds to a reduction in the size, weight, and power input required for eC cooling systems. All these pros in loading via bending can represent a promising approach toward the overcome of key bottlenecks that characterize the realization of elastocaloric systems.

#### 1.4. Aim of the paper and research gap

CHECK TEMPERATURE is the acronym of Controlling the Heating of Electronic Circuits: a Key-approach Through Elastocaloric Materials in a Prototype Employing them as Refrigerants of an AcTive Ultrasmall Refrigerator. The CHECK TEMPERATURE project intends to develop the first elastocaloric device for electronic circuits cooling. Even if it belongs to small-scale, differently from the already existing ones, we intend to develop a device basing on the AeR as thermodynamical cycle and bending as loading/unloading mode.

The paper intends to introduce the results of a numerical analysis for the development of the CHECK TEMPERATURE prototype, through which optimizing both the geometrical configuration for the assembly of the elastocaloric material in the channel and the working conditions.

The main novelties introduced in this paper are:

 the field of application: as, a matter of fact, interesting but never touched before by elastocaloric refrigeration is the electronic circuits cooling field. Many are the application where a more advanced cooling system is required to avoid the unconditional rising of the working temperatures of the devices. As a consequence of temperature rising the failure probability of electronic circuits increases

- exponentially. None of the elastocaloric devices previously reviewed is explicitly devoted toward this field.
- The accuracy and completeness of the numerical model and the analysis perpetuated. Most of the models on elastocaloric systems developed and presented to scientific community are 1D [27] and in literature are not published studies drawing wide maps of performances on elastocaloric devices on small scale and at the same time optimizing the geometrical design and the operative parameters.
- There are no elastocaloric devices based on AeR and bending, already developed and presented in literature.

#### 2. The check temperature project

The project has as final goal the design and manufacturing of an elastocaloric device oriented toward the cooling of electronic circuits. In Fig. 5 the concept of the prototype operation is shown.

From Fig. 5 one can observe, through a longitudinal view, two channels where the wires of elastocaloric materials are lodged. A bar regulating the bending operation is located in the middle of the channels, thus providing the loading/unloading of the wires through up and down vertical translation. The two channels interact themselves only through the loading via bending: when a channel sees loaded their wires, in the other one the elastocaloric material is experimenting the unloading step. The steps are occurring in opposite side so to double the frequency of the device. The heat transfer fluid is air and it provides the rejection of the heat associated to the latent heat of the eC material while it is martensite. Dually the HTF absorbs heat while the eC is austenite.

If the top channel is loaded, in the bottom one the eC is unloaded and the HTF flows in the opposite direction of the upper one. When the bar falls upon the bottom channel, it would result loaded while the topper would be unloaded. Consequently, through a valve system and conveyors of fluxes the directions where HTF flows will be reversed. This allows the two channels to have their AeR cycle. In Fig. 6 the detailed placement of the wires is reported.

 $Ni_{50.8}Ti_{49.2}$  alloy [62] is the elastocaloric material employed in the device. Each wire has 0.5 mm as diameter whereas the length and the placement (i.e. the distance between two consecutive wires in the channel) are parameters investigated in this paper. The elastocaloric details of the  $Ni_{50.8}Ti_{49.2}$  alloy are listed in Table 1.

#### 3. The numerical tool of check temperature

#### 3.1. Geometric design

In this section the numerical model of CHECK TEMPERATURE is introduced; the model has a 2-D design [69,70]. The model reproduces only one of the two channels, since they are not thermodynamically connected as well as the behaviour of one is completely reliable in the other one. As already mentioned in the previous section, the presence of

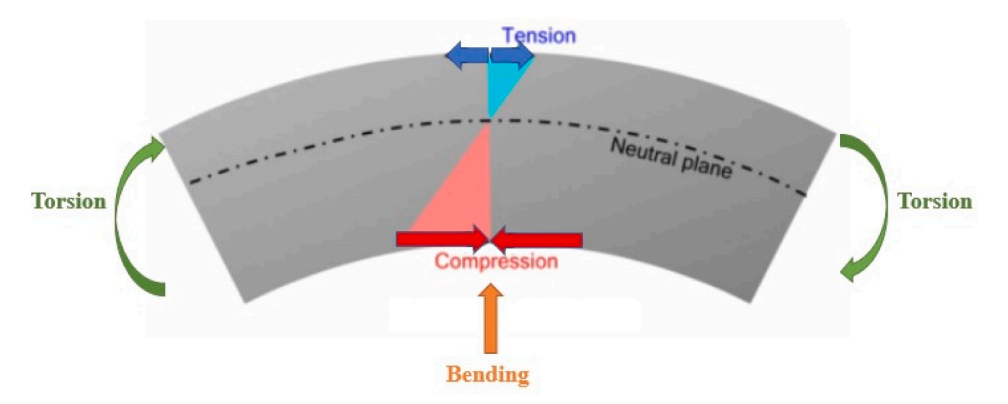


Fig. 4. The main ways to load SMAs.

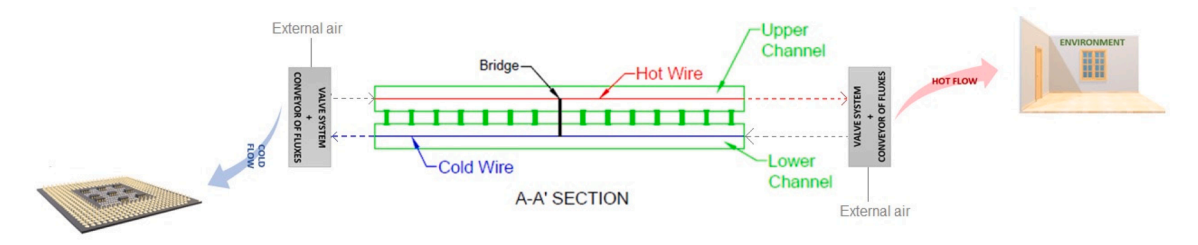


Fig. 5. The design of CHECK TEMPERATURE.

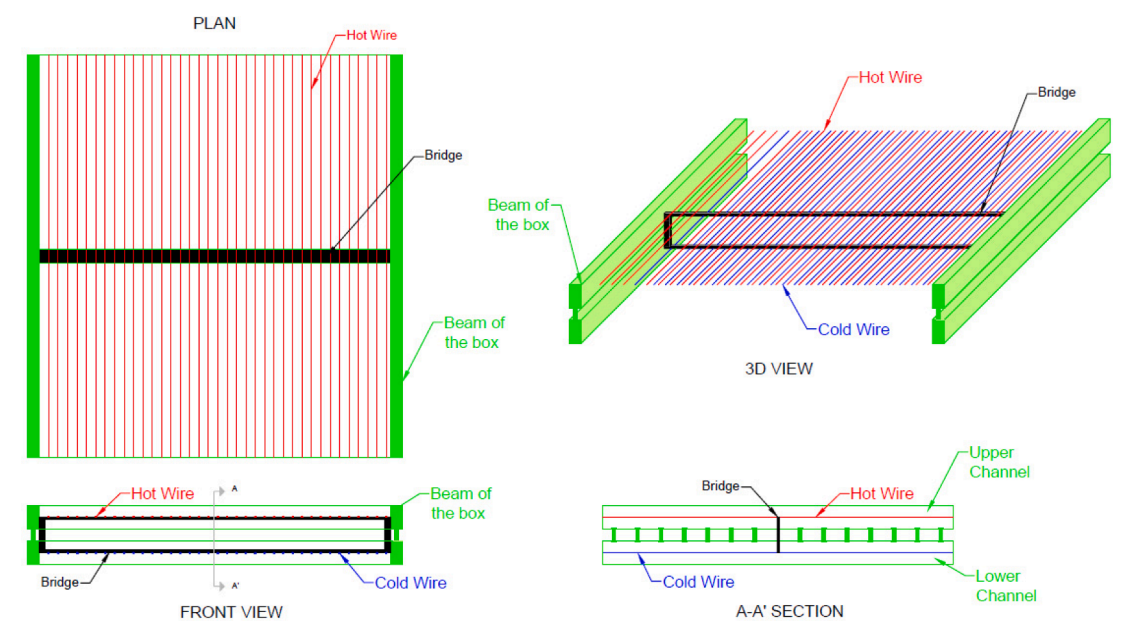


Fig. 6. The design of CHECK TEMPERATURE.

**Table 1**The elastocaloric characteristics of Ni<sub>50.8</sub>Ti<sub>49.2</sub> [68].

Temperature (°C)	$\Delta T_{ad}$ (°C) ( $\epsilon = 6$ % s	bending s.r = 0.025 s $^{-1}$ T <sub>ref</sub> = 20 °C)	Latent Heat bending (J/g)	
	Loading	Unloading	Loading	Unloading
$\begin{aligned} &A_f = -14.5 \\ &A_s = -25.5 \\ &M_s = -38.1 \\ &M_f = -51.2 \end{aligned}$	13.0	11	16.9	14.6

two channels has an influence on the operation frequency: since in the two channels opposite steps of the AeR cycle occur at the same time, the operation frequency of the whole device CHECK TEMPERATURE is twotimes the frequency of each channel. The choice of bending as forcing mode is confirmed by the results of a preliminary study [69] on this device where the energy performances obtainable if the wires are forced through a tensile or a bending mechanism were numerically investigated by means of the development of 2D models based on finite element method. In the study two possible designs of CHECK TEMPERATURE formed by 240 cylindrical wires (120 per channel) of  $Ni_{50.8}Ti_{49.2}$  with D = 0.5 mm as diameter and L = 30 cm as length were analysed considering tensile and bending loading. The final conclusion of the study was that "based on the results obtained it is possible to assess that a small size chiller based on the caloric effect is suitable for cooling the electronic circuits and that the configuration based on bending is the most promising" [69]. The results of [69] are the starting point for the investigation reported in the presented paper where the device loaded via bending is tested while mounting wires of different lengths and distances between

two consecutive wires (according to the lodgement shown in Fig. 6). On the other side choice of the value for the diameter agrees with the conclusions carried out by a previous 2-D investigation [62] on the convective heat exchange between elastocaloric wires and air.

#### 3.2. The mathematical model and boundary conditions

The CHECK TEMPERATURE prototype is designed so that each channel experiments cyclically the four steps of the AeR cycle. Indeed, the supporting mathematical model of the device must guarantee the reproducibility of the four steps: loading, heat releasing through fluid flowing, unloading, heat absorption through fluid flow. In the introduced model the following assumption have been taken:

- isotropy of the elastocaloric material;
- velocity values confined in a range ensuring the fluid blowing laminar;
- neglection of heat transfer due to thermal irradiation;
- thermal insulation of the wrapper with respect to the environment to avoid undesired heat exchanges;
- incompressibility of the fluid;
- not considering viscous dissipation.

Different are the steps of the AeR cycle to be modelled so different are the coupled governing equation systems. During the fluid flow processes (II and IV steps of the AeR cycle) the stress is not changing so there are no phenomena related to eCE, i.e. the governing equations are the Navier-Stokes and the energy equations for the fluid (air) and the solid (SMA):

$$\begin{cases} \frac{\partial u}{\partial x} + \frac{\partial v}{\partial y} = 0 \\ \frac{\partial u}{\partial t} + u \frac{\partial u}{\partial x} + v \frac{\partial u}{\partial y} = -\frac{1}{\rho_{air}} \frac{\partial p}{\partial x} + \nu \left( \frac{\partial^2 u}{\partial x^2} + \frac{\partial^2 u}{\partial y^2} \right) \\ \frac{\partial v}{\partial t} + u \frac{\partial v}{\partial x} + v \frac{\partial v}{\partial y} = -\frac{1}{\rho_{air}} \frac{\partial p}{\partial y} + \nu \left( \frac{\partial^2 v}{\partial x^2} + \frac{\partial^2 v}{\partial y^2} \right) \\ \frac{\partial T_{air}}{\partial t} + u \frac{\partial T_{air}}{\partial x} + v \frac{\partial T_{air}}{\partial y} = \frac{k_{air}}{\rho_{air} c_{air,p}} \left( \frac{\partial^2 T_{air}}{\partial x^2} + \frac{\partial^2 T_{air}}{\partial y^2} \right) \\ \frac{\partial T_{SMA}}{\partial t} = \frac{k_{SMA}}{\rho_{SMA} c_{SMA,p}} \left( \frac{\partial^2 T_{SMA}}{\partial x^2} + \frac{\partial^2 T_{SMA}}{\partial y^2} \right) \end{cases}$$

$$(3)$$

The boundary conditions coupled to eqs. system (3) are the following:

- fluid-dynamically, a velocity vector  $\vec{v}$  models opportunely the direction of the air since it is positive if the HTF crosses the channel from left to right; negative in the dual condition.
- Thermally, the interaction between the AeR regenerator and the surrounding environment is regulated by Dirichlet boundary conditions, i.e. in the T<sub>env</sub> as temperature of entering air is imposed on the left side/right side depending on whether the air blows in the II/IV steps of the AeR cycle.

In the loading and unloading steps the air is not flowing and these processes occur adiabatically, i.e. the coupled boundary condition in these processes is thermal insulation applied to all the boundaries of the channel. Indeed, the eCE manifests as a  $\Delta T_{ad\_load}$  and  $\Delta T_{ad\_unload}$  respectively, to which are associated loading and unloading latent heat values, as listed in Table 1. The set of equations that mathematically describes these steps is:

$$\begin{cases}
\frac{\partial T_{air}}{\partial t} + u \frac{\partial T_{air}}{\partial x} + v \frac{\partial T_{air}}{\partial y} = \frac{k_{air}}{\rho_{air} C_{air,p}} \left( \frac{\partial^2 T_{air}}{\partial x^2} + \frac{\partial^2 T_{air}}{\partial y^2} \right) \\
\frac{\partial T_{SMA}}{\partial t} = \frac{k_{SMA}}{\rho_{SMA} C_{SMA,p}} \left( \frac{\partial^2 T_{SMA}}{\partial x^2} + \frac{\partial^2 T_{SMA}}{\partial y^2} \right) + g_{bend}
\end{cases} (4)$$

where  $g_{bend}$  is a heat source [W/m<sup>3</sup>] due to the elastocaloric effect and it accounts both the loading and unloading as:

$$g_{bend} = g_{load} * a n_1(t) + g_{unload} * a n_2(t)$$
(5)

where  $an_1(t)$  and  $an_2(t)$  are two analytical functions reproducing customized square waves functions, displayed in Fig. 7, so to let the eCE manifesting as positive/negative heat source depending on loading/unloading processes.

The amplitudes of the above-mentioned square waves are given by:

$$g_{load} = \rho_{SMA} (\Delta H_{load} + w_{load}) \dot{\xi}_{M} \tag{6}$$

$$g_{unload} = \rho_{SMA} (\Delta H_{unload} + w_{unload}) \dot{\xi}_M \tag{7}$$

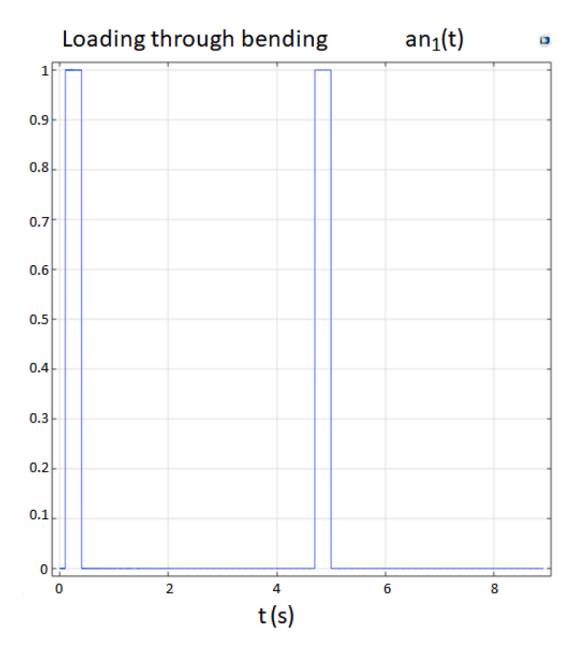
As underlined in eqs. (6)–(7), due to thermal hysteresis of the stressdrive cycle, different are the values of latent heat for loading and unloading, as well as the work required [71]. According to Tusek et al. [72] it is possible to estimate the net-work as the area enclosed by the hysteresis cycle defined by the transformations in s-T plane as:

$$w_{net} = w_{load} - w_{unload} \tag{8}$$

The martensite volume fraction  $\dot{\xi}_M$  is instantaneously estimated through the relation (9):

$$\dot{\xi}_M = -\xi_M \psi^{MA}(T_{SMA}, \sigma) + \xi_A \psi^{AM}(T_{SMA}, \sigma) \tag{9}$$

where, postulating that when the SMA is fully austenite  $\xi_A=1$  and  $\xi_M=0$ ; and when the SMA is fully martensite  $\xi_A=0$  and  $\xi_M=1$ , the following relation is anyhow valid for every moment of the AM-MA



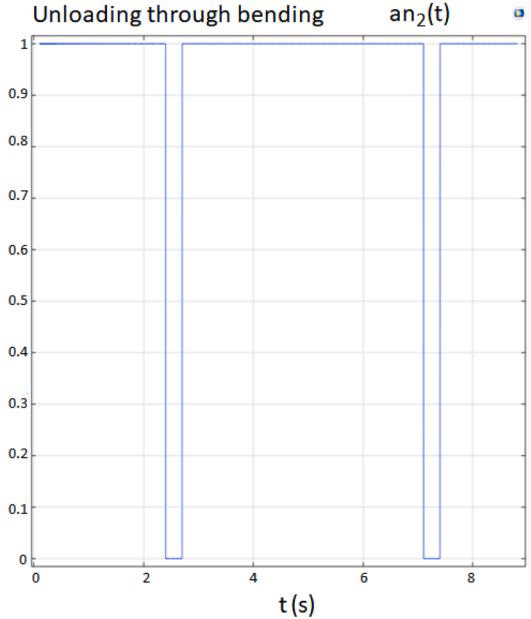


Fig. 7. Timeline on loading/unloading through bending on the wires of one of the two channels.

transformations:

$$\xi_A + \xi_M = 1 \tag{10}$$

Moreover, the transition probabilities  $\psi^{MA}$  and  $\psi^{AM}$  are computed through the approach proposed by Qian et al. [73] basing on the kinetic model of the single crystal [74]:

$$\psi^{AM}(T_{SMA}, \sigma) = \frac{1}{\theta} \frac{\exp\left(-a\left(\frac{\sigma_{AM}(T_{SMA}) - \sigma}{E_A}\right)^2\right)}{\operatorname{erf}\left(\sqrt{a} \frac{\sigma_{AM}(T_{SMA}) - \sigma}{E_A}\right) + \operatorname{erf}\left(\sqrt{a} \frac{\sigma_{AM}(T_{SMA}) + \sigma}{E_A}\right)}$$
(11)

$$\Psi^{MA}(T_{SMA}, \sigma) = \frac{1}{\theta} \frac{\exp\left(-b\left(\frac{\sigma_{MA}(T_{SMA}) - \sigma}{E_M}\right)^2\right)}{\operatorname{erfc}\left(\sqrt{b} \frac{\sigma_{MA}(T_{SMA}) - \sigma}{E_M}\right)}$$
(12)

*a* and *b* are quantities grouping the following relations:

$$a = \frac{E_A V_{SMA}}{2BT_{SMA}} \tag{13}$$

$$b = \frac{E_M V_{SMA}}{2BT_{SMA}} \tag{14}$$

#### 3.3. Meshing and solving

The equations systems (3) and (4) are solved through the FEM method. According to FEM approach the domain has been divided into triangular elements, following free triangular meshing as visible in Fig. 8 where a zoom on three wires and channels is reported.

The resolution of the equations of the FEM model has been done through a time dependent solver that, due to its stability and affordability, utilizes the implicit BDF (Backward Differentiation Formula) as time step procedure, so to work with equations presenting accuracy from 1 (named as the backward Euler method) to 5. The optimum in terms of accuracy would be to employ high order BDF whenever it is possible and lower order BDF only when stability of the resolution must be kept. The latter strategy is called Free time stepping allowing the solver to set larger or reduced time steps to satisfy the required tolerances. In fact, the solver tries to calculate with the largest possible time step, but, when the solution is characterized by high-slope gradients the relative and absolute tolerances could not be respected anymore and, consequently, the size of the timestep is reduced as required. The values of the absolute and relative tolerances fixed for the solver are 5\*10<sup>-4</sup> and 1\*10<sup>-2</sup>, respectively.

A grid independence study has been perpetuated in a previous our study [69] comparing three different grids, i.e. different number and dimensions of the triangular elements. The consistent grid is formed by 137,084 vol triangular elements, and it ensures a maximum deviation in the temperature lower than 0.03 K. The model has been validated experimentally: the methodology and the accuracy are results of an our already published study [69].

AeR cycles is repeated, i.e. steps are simulated cyclically, as until achieving the cyclicity:

$$\delta = \max \left\{ T(x, y, 0 + nt_{cycle}) - T(x, y, t_{cycle} + nt_{cycle}) \right\} \langle \overline{\varepsilon}$$
 (15)

#### 4. Operative conditions

An accurate campaign of numerical tests has been carried out through the above-mentioned CHECK TEMPERATURE 2D Model. The device is made of wires of  $Ni_{50.8}Ti_{49.2}$ : two different length values (20 cm and 30 cm) have been tested as well as two different distances stacked by the placement of two consecutive wires (0.5 mm and 1.2 mm). As

mentioned before, the  $Ni_{50.8}Ti_{49.2}$  is the shape memory alloy employed as solid-state refrigerant of the device, on which a 6 % strain with a strain rate of 0.025 s<sup>-1</sup> is forced for loading unloading cycles through bending.

The choice of the amount and the NiTi alloy composition ensures that the maximum theoretically cooling power achievable by the prototype thus conceived is given by the following relation:

$$\dot{Q}_{MAX} = m_{SMA} f_{MAX} \Delta H \tag{16}$$

The heat transfer flow is the air that enters the device at the environment temperature of 20  $^{\circ}$ C. Such choice allows, in a preliminary configuration of the CHECK TEMPERATURE, to operate without a cold and a hot heat exchanger.

The  $f_{MAX}$  is a parameter that comes from the period of the AeR cycle and, more specifically, from the time for loading/unloading and fluid-flow steps.

The fluid-flow steps must be accurately set after a preliminary evaluation of the Biot number of the elastocaloric wire in the prototype, defined as:

$$Bi = \frac{hV_{wire}}{k_{SMA}Surf_{wire}} \tag{17}$$

The convective heat transfer coefficient (h) can be evaluated through literature correlation or numerically. In this analysis we opted for the second option, and we calculated h through the above introduced numerical model as:

$$h(x) = \frac{\dot{q}_c(x)}{T_{wire}(x) - T_{air}(x)}$$
(18)

Given the small diameter of the wire (0.5 mm) and the low convective heat transfer coefficient proper of air, this choice ensures the Bi number being always below 0.1.

The heat exchange so is regulated by  $\tau$  that the time-dependent constant:

$$\tau = \frac{\rho_{SMA}c_{SMA}V_{wire}}{hSurf_{wire}} = \frac{\rho_{SMA}c_{SMA}D_{wire}}{4h}$$
(19)

Indeed, the choice of the fluid flow time must be considered respecting the minimum fixed by the time-dependent constant: a  $3-4~\tau$  time is required to ensure the convective heat exchange completely occurs.

The range of velocity values for the air entering the channel in the fluid flow steps is:

$$v_{air} = [3; 5; 7; 9; 11]s (20)$$

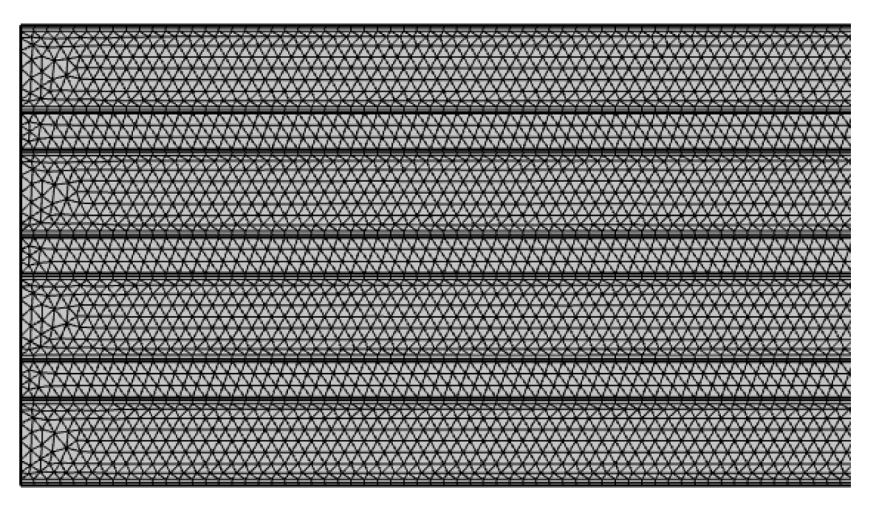


Fig. 8. Timeline on loading/unloading through bending on the wires of one of the two channels.

From this, there is a maximum frequency (related to one channel) for each flow velocity and the values have been reported in Table 2.

Indeed, the time for fluid flow has been chosen respecting the above constraints (3–4) and the set of values investigated are:

$$t_{fluid} = [4.0; 6.0; 8.0; 10.0]s (21)$$

The energy performances of the device have been evaluated according to the following formulas:

$$\Delta T_{span,cold} = \left( T_{env} - \frac{1}{t_{cycle}} \int_{t_{load} + t_{fluid} + t_{unload} + nt_{cycle}}^{t_{cycle}} T_{air}(0, y, t) dt \right)$$
(22)

$$\Delta T_{span,global} = \left(\frac{1}{t_{cycle}} \int_{t_{load}+t_{fluid}+nt_{cycle}}^{t_{load}+t_{fluid}+nt_{cycle}} T_{air}(L, y, t) dt - \frac{1}{t_{cycle}} \int_{t_{load}+t_{fluid}+t_{unload}+nt_{cycle}}^{t_{cycle}+nt_{cycle}} T_{air}(0, y, t) dt \right)$$
(23)

$$\dot{Q}_{cool} = \frac{1}{t_{cycle}} \int_{t_{load} + t_{fluid} + t_{unload} + nt_{cycle}}^{t_{cycle} + nt_{cycle}} \dot{m}_{air} c_{air} (T_{env} - T_{air}(0, y, t)) dt$$
(24)

The temperature span on cold  $(\Delta T_{span,cold})$  is a measure of the jump between the temperature of the external air entering the system and the temperature of the cold flux exiting from the device, in an entire cycle. The temperature span global  $(\Delta T_{span,global})$  accounts for the global span on the temperatures of the air between the hot flux and cold flux exiting from the device, in an entire cycle.

 $\dot{Q}_{cool}$  is the cooling power and in our study  $T_{env}$  is 293 K. The coefficient of performance is defined as:

$$COP = \frac{\dot{Q}_{cool}}{\dot{w}} \tag{25}$$

where  $\dot{W}$  is the global expense paid for the operation of the device. This contribution is the sum of the mechanical power per unit of time-related to the loading of the wires, the mechanical expense for air motion (according to the pressure losses).

#### 5. Results

This section summarizes the energy performances of the CHECK TEMPERATURE device, working under the operating conditions listed in the previous section. The data plotted were extrapolated by the simulations performed through the numerical model operating under steady-state conditions of the AeR cycle, i.e. with the satisfaction of the cyclicity criterion.

The first geometrical parameter under investigation has been the distance d stacked between the placement of two consecutive wires along the channels of the device. Specifically, as first step, at fixed length of the wire (20 cm), the influence on the energy performances of the device of two different distances ( $d=0.5~\mathrm{mm}$  and  $d=1.2~\mathrm{mm}$ ) has been considered.

Fig. 9 plots the *temperature span global* ( $\Delta T_{span,global}$ ) vs frequency of the device ( $f_{CHECK}$ ) parametrized for the inlet velocity of the air, according to the investigation ranges of eqs. (20) and (21), considering d

**Table 2**Setting parameters and maximum frequency for channel and device.

Velocity (m/s)	T (s)	3τ (s)	4τ (s)	f <sub>MAX,CHANNEL</sub> (Hz)	f <sub>MAX,CHECK</sub> (Hz)
3.0	1.40	4.2	5.6	0.17	0.34
5.0	1.08	3.24	4.32	0.21	0.42
7.0	0.91	2.73	3.64	0.25	0.5
9.0	0.81	2.43	3.24	0.27	0.54
11.0	0.73	2.19	2.92	0.30	0.60

= 0.5 mm and d=1.2 mm. There is always an optimal frequency that maximises the temperature span, for fixed velocity and distance. The measured  $\Delta T_{span,global}$  are larger if the wires are placed with d=0.5 mm, on equal operative conditions with peaks at 0.122 Hz for each tested v and an absolute maximum of 23.9 K with a velocity of 3 m s<sup>-1</sup>.

If the distance between the wires is 1.2 mm, the maximum falls at different frequencies by varying the velocities. The maximum  $\Delta T_{span}$ ,  $g_{lobal}$  is 20.1 K, registered 0.239 Hz and 3 m s<sup>-1</sup>. By comparing the two geometric configurations one can evaluate a medium increment of +55 % for the  $\Delta T_{span,global}$  plotted in Fig. 9(a).

Fig. 10 plots the cooling power of the device vs frequency parametrized for air velocity where the wires are distanced at: (a) 0.5 mm; (b) 1.2 mm. The greater is v the higher are the cooling power values because of the growing fluid flow rate for increasing velocity values. If fixed is the velocity  $\dot{Q}_{cool}$  has peak at frequencies different with  $\Delta T_{span}$  ones, i.e. there is trade-off in maximizing  $\Delta T_{span}$  and  $\dot{Q}_{cool}$ . The maximum  $\dot{Q}_{cool}$  evaluated are 68.1 W and 49.0 W at 0.096 Hz and 11 m s<sup>-1</sup>, respectively with d = 0.5 mm and 1.2 mm. The comparison between the two configurations gives + 30 % as medium increment in cooling power registered for the geometry with d = 0.5 mm.

The COP is plotted as a function of the cycle frequency parametrized for air velocity for d = 0.5 in Fig. 11(a); d = 1.2 mm in Fig. 11(b).

At fixed frequency the COP is an increasing function of the air velocity (except at very low value of the frequency) with maximum of 6.8 (v = 9 m s<sup>-1</sup>; f = 0.096 Hz) and 5.2 (v = 7 m s<sup>-1</sup>; f = 0.096 Hz) respectively for d = 0.5 mm and d = 1.2 mm. At fixed velocity the COP decreases with the growing cycle frequency. 3 is the acceptable threshold value above which the device under test is intended to work. This implies the device operate at smaller frequency, since the time needed to get a complete convective heat exchange between the wires and air is a strong discriminant. Smaller cycle frequencies translate in larger times for convective heat transfer. Anyhow since that the COP of the geometry with wires placed at 0.5 mm, always overperforms of +30 % the 1.2 mm configuration, from the figures one can observe that, always considering 3 as threshold value, the former (d = 0.5 mm) allows the device to work up to higher frequencies (0.161 Hz) rather than the latter (1.2 mm) where the limit is 0.122 Hz.

Basing on all the considerations carried out from Figs. 9-10-11, one can conclude that the device mounting wires with length of 20 cm stacked at a distance 0.5 mm globally confers higher energy performances both in terms of temperature span, cooling power and COP.

As second step of the investigation, considering d=0.5 mm the employment of wires with L=20 cm and L=30 cm is compared, considering equal the number of wires (240), i.e. different mass of the elastocaloric material employed in the device: 61.23 g and 91.85 g, respectively if L=20 cm or 30 cm.

Fig. 12 report the temperature span evaluated on cold (according to eq. (22)) as a function of time for fluid flow parametrized for air velocity for the two geometries where d =0.5 mm and (a) L =20 cm, (b) L =30 cm. Figures clearly show a different behaviour for the two geometries: for each velocity the temperature span of L =20 cm configuration is an increasing function of fluid flow time whereas for longer wires (L =30 cm) it reaches a peak and then it start falling. The augmentation of the length has a slight, not remarkable effect on temperature span since the values are comparable each other (+4 % as medium increment).

Fig. 13 plots the cooling power as a function of air flow time parametrized for v with: (a) L=20 cm, (b) L=30 cm as length of the wires. On equal frequency, i.e. air flow time, the cooling power is an increasing function of air velocity since the mass flow rate also increases. Therefore, again there is a trade-off between  $\Delta T_{SPAN}$  and cooling power. For the configuration with L=20 cm  $\dot{Q}_{cool}$  increases with the air flow time whereas for L=30 cm it reaches a peak at the same frequency where the peak of  $\Delta T_{SPAN}$  falls. The higher the frequencies, the slighter the deviations calculated (the smallest is +~10~% mean value at f=0.238~Hz, i.e. 4 s as air flow time). The maximum deviation (+20 %

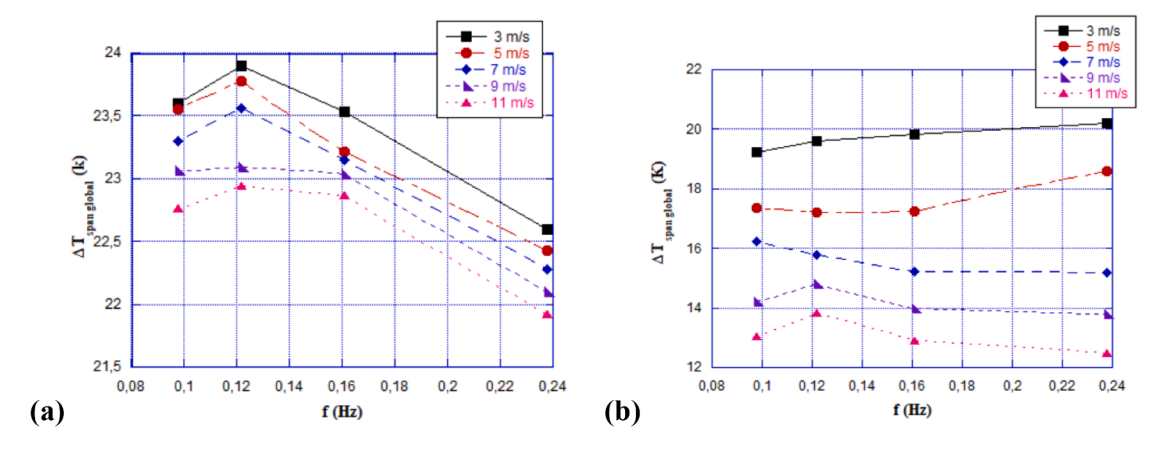


Fig. 9. Temperature span global vs frequency of the device parametrized for air velocity for wires placed at: (a) 0.5 mm; (b) 1.2 mm.

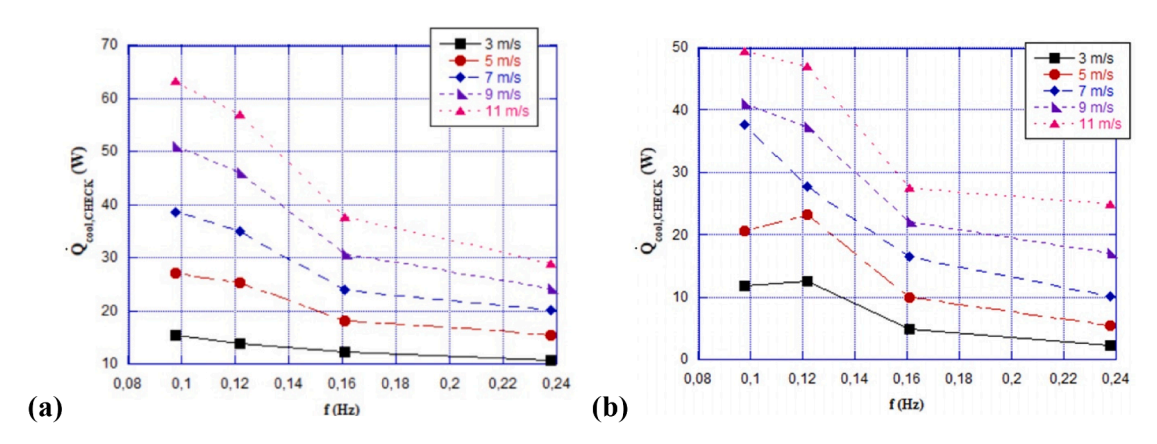


Fig. 10. Cooling power vs frequency of the device parametrized for fluid velocity for wires placed at: (a) 0.5 mm; (b) 1.2 mm.

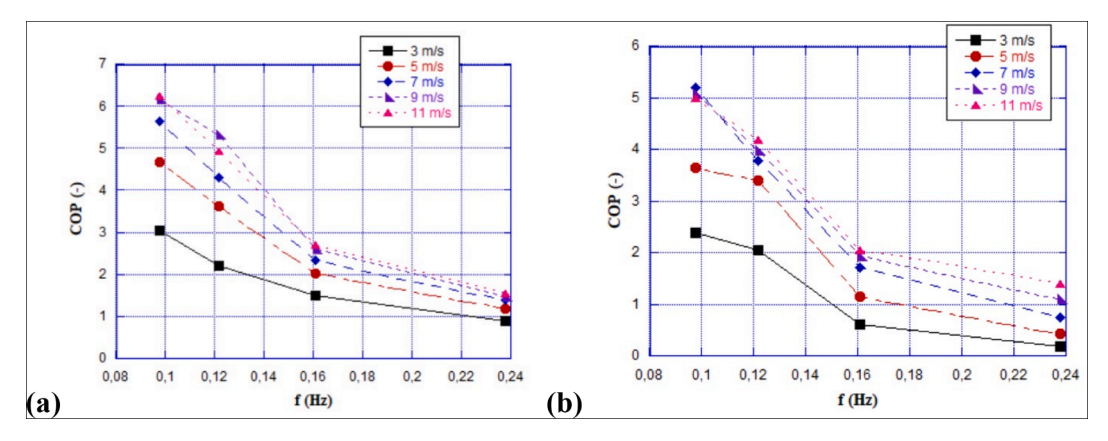


Fig. 11. COP vs frequency of the device parametrized for fluid velocity for wires placed at: (a) 0.5 mm; (b) 1.2 mm.

mean value) has been evaluated for f=0.098~Hz (10 s as air flow time). Fig. 14 show the coefficient of performance vs fluid flow speed parametrized for the time for fluid for: (a) L=20~cm, (b) L=30~cm as length of the wires. For both the configurations investigated COP increases with air flow speed, as happening for cooling power; this is due to the preponderance of the mechanical power needed for the loading of the wires with respect to the contribution related to the fluid motion, on the total work per unit time. The latter is a function of air speed whereas the former is fixed. Moreover, on equal fluid flow velocity, COP values augment with period of the cycle. In all the working points the COP calculated for the L=30~cm configuration is always greater than L=20~cm (from a minimum of +11~% to a maximum of +46~%). To make the

device operating in working points characterized by acceptable COP (not under 3), the time for fluid flowing must necessarily be greater than 6 s. The highest COPs are calculated for  $t=10\,s$  and high velocities (9 m s $^{-1}$  and 11 m s $^{-1}$ ); indeed, under these working conditions the COP values belong to the range 6.0–6.5.

#### 6. Conclusion

In this paper CHECK TEMPERATURE, the design of the first elastocaloric device for the cooling of electronic circuits is investigated through a 2D numerical model. From the results of the investigations the following conclusions can be summarized as:

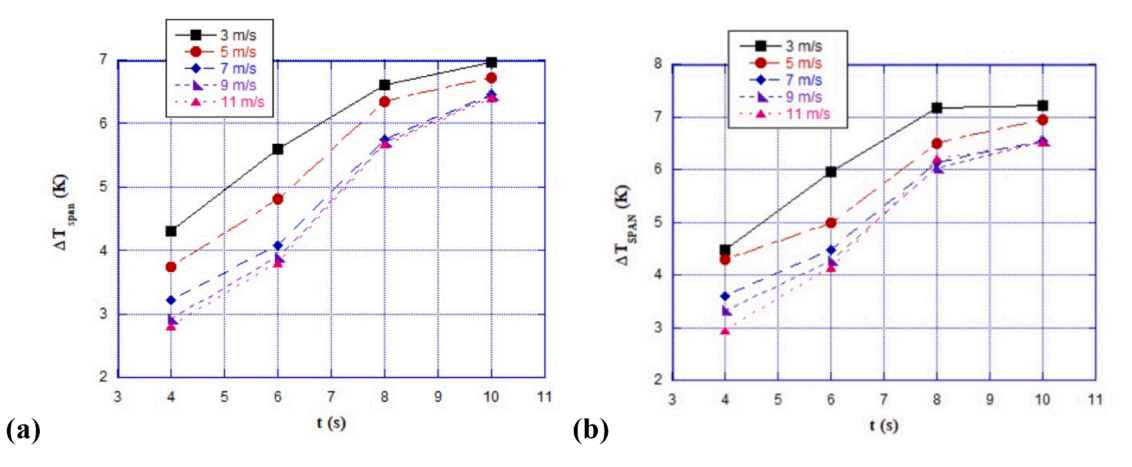


Fig. 12. Temperature span on cold vs time for fluid flow parametrized for air velocity for wires length of: (a) 20 cm; (b) 30 cm, with d = 0.5 mm.

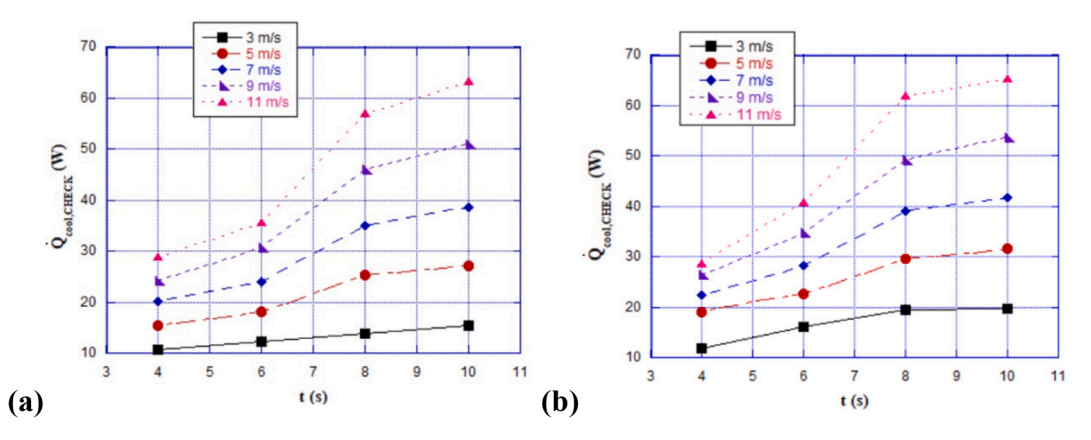


Fig. 13. Cooling power vs time for fluid flow parametrized for fluid velocity for wires length of: (a) 20 cm; (b) 30 cm, with d = 0.5 mm.

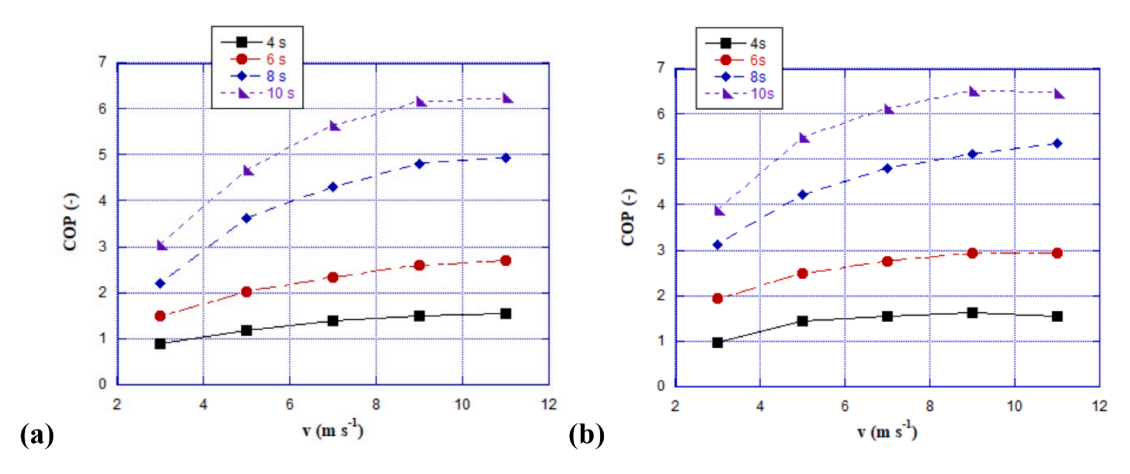


Fig. 14. COP vs time for fluid velocity parametrized for fluid flow time for wires length of: (a) 20 cm; (b) 30 cm, with d = 0.5 mm.

- The placement of wires stacked at 0.5 mm along the channel is to be preferred than 1.2 mm since temperature span, cooling power and COP are greater, with respectively medium increments of +55 %, +30 %, +30 %, on equal wire length (20 cm) and working conditions.
- Keeping d = 0.5 mm and analysing the influence of the length on the energy performances, +4 % larger temperature span are measured if the length of the wires is 30 cm rather than 20 cm;
- $\bullet$  Cooling powers calculated for the configuration with L =30 cm show a positive deviation ranging from a minimum of +10~% to a
- maximum of +20 % even if both the configurations (L = 20 cm and L = 30 cm) exhibits a maximum larger than 60 W.
- $\bullet$  COPs evaluated for the L = 30 cm configuration are always greater than L = 20 cm, with a deviation ranging from a minimum of +11 % to a maximum of +46 %.
- To make the device operating in working points characterized by acceptable COP (not smaller than 3), the time for fluid flowing must necessarily be greater than 6 s. The highest COPs are calculated for t = 10 s and high velocities (9 m s<sup>-1</sup> and 11 m s<sup>-1</sup>): under these

- working conditions the values belong to the range 6.0–6.5 for both the configurations.
- Keeping constant the number of wires employed in the device (240), the  $L=20\,$  cm configuration needs of 61.23 g of elastocaloric material, whereas  $L=30\,$  cm utilizes 91.85 g.

Basing on the above summarized points,  $d=0.5\,\mathrm{mm}$  is certainly the best distance to place the wires among the investigated. Moreover, even if slightly better are the energy performances coupled with wires 30 cm long, keeping constant the number of wires, the solution where 20 cm is the length of every wire must be preferred since 30 % less elastocaloric material is used with consequent cost saving.

The collected and discussed results confirm the favourability in betting on elastocaloric technology for the application to the field of electronic circuits cooling. The optimized geometrical design conditions have been identified and the device is currently under construction. The next perspective related to the future research work will be the comparison between the experimental results given by the CHECK TEMPERATURE device and the numerical ones. The model will be a useful tool to investigate further points of improvement to be implemented in the experimental device.

#### **Declaration of Competing Interest**

The authors declare the following financial interests/personal relationships which may be considered as potential competing interests: Claudia Masselli reports financial support was provided by University of Naples Federico II Department of Industrial Engineering.

#### Data availability

Data will be made available on request.

#### Acknowledgment

The paper is realized from the project CHECK TEMPERATURE that is financially supported by the 2021 internal grant reserved for Fixed-Term Research of Department of Industrial Engineering, University of Naples Federico II.

#### References

- [1] S. Qian, D. Nasuta, A. Rhoads, Y. Wang, Y. Geng, Y. Hwang, I. Takeuchi, Not-in-kind cooling technologies: a quantitative comparison of refrigerants and system performance, Int. J. Refrig. 62 (2016) 177–192.
- [2] A. Kitanovski, U. Plaznik, U. Tomc, A. Poredoš, Present and future caloric refrigeration and heat-pump technologies, Int. J. Refrig. 57 (2015) 288–298.
- [3] W. Goetzler, R. Zogg, J. Young, C. Johnson, Alternatives to vapor-compression HVAC technology, ASHRAE J. 56 (10) (2014) 12.
- [4] C. Aprea, A. Greco, A. Maiorino, C. Masselli, The use of barocaloric effect for energy saving in a domestic refrigerator with ethylene-glycol based nanofluids: a numerical analysis and a comparison with a vapor compression cooler, Energy 190 (2020), 116404.
- [5] Montreal Protocol on substances that deplete the ozone layer, United Nation Environment Program (UN), New York, NY, USA, 1987.
- [6] Kyoto Protocol to the United Nation Framework Convention on Climate Change, Kyoto, JPN, 1997.
- [7] C. Aprea, A. Greco, A. Rosato, Comparison of R407C and R417A heat transfer coefficients and pressure drops during flow boiling in a horizontal smooth tube, Energ. Conver. Manage. 49 (6) (2008) 1629–1636.
- [8] A. Greco, R. Mastrullo, A. Palombo, R407C as an alternative to R22 in vapour compression plant: an experimental study, Int. J. Energy Res. 21 (12) (1997) 1087–1098.
- [9] C. Aprea, A. Greco, Performance evaluation of R22 and R407C in a vapour compression plant with reciprocating compressor, Appl. Therm. Eng. 23 (2) (2003) 215–227.
- [10] M. Salvia, M. Olazabal, P.A. Fokaides, L. Tardieu, S.G. Simoes, D. Geneletti, D. Reckien, Climate mitigation in the Mediterranean Europe: an assessment of regional and city-level plans, J. Environ. Manage. 295 (2021), 113146.
- [11] Y. Heredia-Aricapa, J.M. Belman-Flores, A. Mota-Babiloni, J. Serrano-Arellano, J. J. García-Pabón, Overview of low GWP mixtures for the replacement of HFC refrigerants: R134a, R404A and R410A, Int. J. Refrig. 111 (2020) 113–123.

- [12] C. Aprea, A. Greco, A. Maiorino, C. Masselli, A. Metallo, HFO1234yf as a drop-in replacement for R134a in domestic refrigerators: a life cycle climate performance analysis, Int. J. Heat Technol. 34 (2) (2016) S212–S218.
- [13] R.C. Pietzcker, D. Stetter, S. Manger, G. Luderer, Using the sun to decarbonize the power sector: the economic potential of photovoltaics and concentrating solar power, Appl. Energy 135 (2014) 704–720.
- [14] B. Wang, J.J. Klemeš, P.S. Varbanov, K. Shahzad, M.R. Kabli, Total Site Heat Integration benefiting from geothermal energy for heating and cooling implementations, J. Environ. Manage. 290 (2021), 112596.
- [15] S. Fähler, Caloric effects in ferroic materials: new concepts for cooling, Energ. Technol. 6 (8) (2018) 1394–1396.
- [16] C. Aprea, A. Greco, A. Maiorino, C. Masselli, Analyzing the energetic performances of AMR regenerator working with different magnetocaloric materials: investigations and viewpoints, Int. J. Heat Technol. 35 (2017) S383–S390.
- [17] V. Franco, J.S. Blázquez, J.J. Ipus, J.Y. Law, L.M. Moreno-Ramírez, A. Conde, Magnetocaloric effect: from materials research to refrigeration devices, Prog. Mater Sci. 93 (2018) 112–232.
- [18] C. Aprea, A. Greco, A. Maiorino, C. Masselli, Energy performances and numerical investigation of solid-state magnetocaloric materials used as refrigerant in an active magnetic regenerator, Therm. Sci. Eng. Prog. 6 (2018) 370–379.
- [19] C. Aprea, A. Greco, A. Maiorino, Modelling an active magnetic refrigeration system: a comparison with different models of incompressible flow through a packed bed, Appl. Therm. Eng. 36 (2012) 296–306.
- [20] Y. Utaka, K. Hu, Z. Chen, Y. Zhao, Application of simple and effective thermal switch for solid-state magnetic refrigeration at room temperature, Appl. Therm. Eng. 155 (2019) 196–205.
- [21] J. He, C. Ya, X. Tang, L. Ma, J. Wu, B. Lu, Numerical study of a cascade cycle for the reciprocating solid-state magnetic refrigerator, Appl. Therm. Eng. (2022), 119695.
- [22] D.J. Silva, B.D. Bordalo, J. Puga, A.M. Pereira, J. Ventura, J.C.R.E. Oliveira, J. P. Araújo, Optimization of the physical properties of magnetocaloric materials for solid state magnetic refrigeration, Appl. Therm. Eng. 99 (2016) 514–517.
- [23] U. Tomc, J. Tušek, A. Kitanovski, A. Poredoš, A new magnetocaloric refrigeration principle with solid-state thermoelectric thermal diodes, Appl. Therm. Eng. 58 (1–2) (2013) 1–10.
- [24] A. Greco, C. Masselli, Electrocaloric cooling: a review of the thermodynamic cycles, materials, models, and devices. Magnetochemistry 6 (4) (2020) 67.
- [25] X. Meng, P. Gong, S. Wang, Y. Zhao, X. Ma, W. Xiong, Simulation study on superposition expansion of belt electrocaloric refrigeration structure, Appl. Therm. Eng. (2022), 119855.
- [26] Q. Li, J. Shi, D. Han, F. Du, J. Chen, X. Qian, Concept design and numerical evaluation of a highly efficient rotary electrocaloric refrigeration device, Appl. Therm. Eng. 190 (2021), 116806.
- [27] S. Qian, Y. Geng, Y. Wang, J. Ling, Y. Hwang, R. Radermacher, J. Cui, A review of elastocaloric cooling: materials, cycles and system integrations, Int. J. Refrig. 64 (2016) 1–19.
- [28] Y. Wu, Y. Liu, S. Qian, Numerical simulation of a foam regenerator for elastocaloric cooling, Appl. Therm. Eng. (2022), 119819.
- [29] L. Yuan, Y. Wang, J. Yu, A. Greco, C. Masselli, S. Qian, Numerical study of a double-effect elastocaloric cooling system powered by low-grade heat, Appl. Therm. Eng. 218 (2023), 119302.
- [30] P. Lloveras, J.L. Tamarit, Advances and obstacles in pressure-driven solid-state cooling: a review of barocaloric materials, MRS Energy Sustain. 8 (1) (2021) 3–15.
- [31] J. Chen, L. Lei, G. Fang, Elastocaloric cooling of shape memory alloys: a review, Mater. Today Commun. 28 (2021), 102706.
- [32] E. Bonnot, R. Romero, L. Mañosa, E. Vives, A. Planes, Elastocaloric effect associated with the martensitic transition in shape-memory alloys, Phys. Rev. Lett. 100 (12) (2008), 125901.
- [33] J. Tušek, K. Engelbrecht, R. Millán-Solsona, L. Manosa, E. Vives, L.P. Mikkelsen, N. Pryds, The elastocaloric effect: a way to cool efficiently, Adv. Energy Mater. 5 (13) (2015), 1500361.
- [34] G. Wehmeyer, T. Yabuki, C. Monachon, J. Wu, C. Dames, Thermal diodes, regulators, and switches: physical mechanisms and potential applications, Appl. Phys. Rev. 4 (4) (2017), 041304.
- [35] K. Klinar, A. Kitanovski, Thermal control elements for caloric energy conversion, Renew. Sustain. Energy Rev. 118 (2020), 109571.
- [36] V. Franco, J.S. Blázquez, B. Ingale, A. Conde, The magnetocaloric effect and magnetic refrigeration near room temperature: materials and models, Annu. Rev. Mat. Res. 42 (2012) 305–342.
- [37] G.V. Brown, Magnetic heat pumping near room temperature, J. Appl. Phys. 47 (8) (1976) 3673–3680.
- [38] A. Greco, C. Aprea, A. Maiorino, C. Masselli, A review of the state of the art of solidstate caloric cooling processes at room-temperature before 2019, Int. J. Refrig. 106 (2019) 66–88.
- [39] Y. Zhang, J. Wu, J. He, K. Wang, G. Yu, Solutions to obstacles in the commercialization of room-temperature magnetic refrigeration, Renew. Sustain. Energy Rev. 143 (2021), 110933.
- [40] C. Aprea, A. Greco, A. Maiorino, C. Masselli, A comparison between electrocaloric and magnetocaloric materials for solid state refrigeration, Int. J. Heat Technol. 35 (1) (2017) 225–234.
- [41] V.K. Pecharsky, K.A. Gschneidner Jr, Advanced magnetocaloric materials: what does the future hold? Int. J. Refrig. 29 (8) (2006) 1239–1249.
- [42] M. Zhou, Y.S. Li, C. Zhang, L.F. Li, Elastocaloric effect and mechanical behavior for NiTi shape memory alloys, Chin. Phys. B 27 (10) (2018), 106501.
- [43] J. Zhang, Y. Zhu, S. Cheng, S. Yao, Q. Sun, Enhancing cooling performance of NiTi elastocaloric tube refrigerant via internal grooving, Appl. Therm. Eng. 213 (2022), 118657.

- [44] H.O. Mosca, G. Bozzolo, M.F. Del Grosso, Atomistic modeling of ternary additions to NiTi and quaternary additions to Ni–Ti–Pd, Ni–Ti–Pt and Ni–Ti–Hf shape memory alloys, Phys. B Condens. Matter 407 (16) (2012) 3244–3247.
- [45] C. Chluba, W. Ge, R. Lima de Miranda, J. Strobel, L. Kienle, E. Quandt, M. Wuttig, Ultralow-fatigue shape memory alloy films, Science 348 (6238) (2015) 1004–1007.
- [46] F. Xiao, T. Fukuda, T. Kakeshita, X. Jin, Elastocaloric effect by a weak first-order transformation associated with lattice softening in an Fe-31.2 Pd (at. %) alloy, Acta Mater. 87 (2015) 8–14.
- [47] R. Bennacer, B. Liu, M. Yang, A. Chen, Refrigeration performance and the elastocaloric effect in natural and synthetic rubbers, Appl. Therm. Eng. 204 (5) (2022), 117938.
- [48] D. Daniel Guyomar, Y. Li, G. Sebald, P.J. Cottinet, B. Ducharne, J.F. Capsal, Elastocaloric modelling of natural rubber, Appl. Therm. Eng. 57 (1–2) (2013) 33–38.
- [49] Z. Xie, G. Sebald, D. Guyomar, Comparison of elastocaloric effect of natural rubber with other caloric effects on different-scale cooling application cases, Appl. Therm. Eng. 111 (25) (2017) 914–926.
- [50] J. Cui, Y. Wu, J. Muehlbauer, Y. Hwang, R. Radermacher, S. Fackler, I. Takeuchi, Demonstration of high efficiency elastocaloric cooling with large ΔT using NiTi wires, Appl. Phys. Lett. 101 (7) (2012), 073904.
- [51] P. Kabirifar, A. Žerovnik, Ž. Ahčin, L. Porenta, M. Brojan, J. Tušek, Elastocaloric cooling: state-of-the-art and future challenges in designing regenerative elastocaloric devices, Strojniski Vestnik/J. Mech. Eng. 65 (11–12) (2019) 615–630.
- [52] S.M. Kirsch, F. Welsch, N. Michaelis, M. Schmidt, A. Wieczorek, J. Frenzel, S. Seelecke, NiTi-based elastocaloric cooling on the macroscale: from basic concepts to realization, Energ. Technol. 6 (8) (2018) 1567–1587.
- [53] F. Bruederlin, H. Ossmer, F. Wendler, S. Miyazaki, M. Kohl, SMA foil-based elastocaloric cooling: from material behavior to device engineering, J. Phys. D: Appl. Phys. 50 (42) (2017).
- [54] F. Bruederlin, L. Bumke, E. Quandt, M. Kohl, Cascaded Sma-film based elastocaloric cooling, in: Proceedings of 20th International Conference on Solid-State Sensors, Actuators and Microsystems & Eurosensors XXXIII (TRANSDUCERS & EUROSENSORS XXXIII), June 2019, pp. 1467–1470.
- [55] R. Snodgrass, D. Erickson, A multistage elastocaloric refrigerator and heat pump with 28 K temperature span, Sci. Rep. 9 (1) (2019) 1–10.
- [56] H. Ossmer, C. Chluba, S. Kauffmann-Weiss, E. Quandt, M. Kohl, TiNi-based films for elastocaloric microcooling—fatigue life and device performance, APL Mater. 4 (6) (2016), 064102.
- [57] Y. Chen, Y. Wang, W. Sun, S. Qian, J. Liu, A compact elastocaloric refrigerator, Innovation 3 (2) (2022), https://doi.org/10.1016/j.xinn.2022.100205.
- [58] Ž. Ahčin, S. Dall'Olio, A. Žerovnik, U.Ž. Baškovič, L. Porenta, P. Kabirifar, J. Tušek, High-performance cooling and heat pumping based on fatigue-resistant elastocaloric effect in compression, Joule 6 (10) (2022) 2338–2357.

- [59] L. Ianniciello, K. Bartholomé, A. Fitger, K. Engelbrecht, Long life elastocaloric regenerator operating under compression, Appl. Therm. Eng. 202 (2022), 117838.
- [60] N. Emaikwu, D. Catalini, J. Muehlbauer, Y. Hwang, I. Takeuchi, R. Radermacher, Experimental investigation of a staggered-tube active elastocaloric regenerator, Int. J. Refrig. (2022).
- [61] L. Cirillo, A.R. Farina, A. Greco, C. Masselli, The optimization of the energy performances of a single bunch of elastocaloric elements to be employed in an experimental device, Therm. Sci. Eng. Prog. 27 (2022), 101152.
- [62] L. Cirillo, A.R. Farina, A. Greco, C. Masselli, Numerical optimization of a single bunch of NiTi wires to be placed in an elastocaloric experimental device: preliminary results, Magnetochemistry 7 (5) (2021) 67.
- [63] L. Ianniciello, K. Bartholomé, A. Fitger, K. Engelbrecht, Long life elastocaloric regenerator operating under compression, Appl. Therm. Eng. 202 (5) (2022), 117838.
- [64] K. Zhang, G. Kang, Q. Sun, High fatigue life and cooling efficiency of NiTi shape memory alloy under cyclic compression, Scr. Mater. 159 (2019) 62–67.
- [65] J. Chen, K. Zhang, Q. Kan, H. Yin, Q. Sun, Ultra-high fatigue life of NiTi cylinders for compression-based elastocaloric cooling, Appl. Phys. Lett. 115 (9) (2019), 093902.
- [66] S. Qian, L. Yuan, H. Hou, I. Takeuchi, Accurate prediction of work and coefficient of performance of elastocaloric materials with phase transformation kinetics, Sci. Technol Built Environ. 24 (6) (2018) 673–684.
- [67] D.J. Sharar, J. Radice, R. Warzoha, B. Hanrahan, A. Smith, Low-force elastocaloric refrigeration via bending, Appl. Phys. Lett. 118 (18) (2021), 184103.
- [68] M. Zhou, Y. Li, C. Zhang, S. Li, E. Wu, W. Li, L. Li, The elastocaloric effect of Ni50.8Ti49.2 shape memory alloys, J. Phys. D: Appl. Phys. 51 (13) (2018), 135303.
- [69] L. Cirillo, A. Greco, C. Masselli, Development of an electronic circuit cooling system using elastocaloric effect: a FEM comparison among different configurations, Appl. Therm. Eng. 219 (2023), 119463.
- [70] X. Li, S. Cheng, Q. Sun, A compact NiTi elastocaloric air cooler with low force bending actuation, Appl. Therm. Eng. 215 (2022), 118942.
- [71] H. Ossmer, F. Lambrecht, M. Gültig, C. Chluba, E. Quandt, M. Kohl, Evolution of temperature profiles in TiNi films for elastocaloric cooling, Acta Mat. 81 (2014) 9, 20
- [72] J. Tušek, K. Engelbrecht, L. Mañosa, E. Vives, N. Pryds, Understanding the thermodynamic properties of the elastocaloric effect through experimentation and modelling, Shape Memory Superelasticity 2 (4) (2016) 317–329.
- [73] S. Qian, L. Yuan, J. Yu, G. Yan, Numerical modeling of an active elastocaloric regenerator refrigerator with phase transformation kinetics and the matching principle for materials selection, Energy 141 (2017) 744–756.
- [74] O. Heintze, A computationally efficient free energy model for shape memory alloys: experiments and theory, Thesis, North Carolina State University, 2005.